


Article

Reaction Mechanism of Pyrolysis and Combustion of Methyl Oleate: A ReaxFF-MD Analysis

Yu Wei ^{1,2}, Xiaohui Zhang ^{1,2,*}, Shan Qing ¹ and Hua Wang ^{1,2} ¹ Faculty of Metallurgy and Energy Engineering, Kunming University of Science and Technology, Kunming 650093, China² State Key Laboratory of Complex Nonferrous Metal Resources Clean Utilization, Kunming University of Science and Technology, Kunming 650093, China

* Correspondence: xiaohui.zhang@kust.edu.cn

Abstract: As an emerging environmentally friendly fuel, biodiesel has excellent fuel properties comparable to those of petrochemical diesel. Oleic acid methyl ester, as the main component of biodiesel, has the characteristics of high cetane number and low emission rate of harmful gases. However, the comprehensive chemical conversion pathway of oleic acid methyl ester is not clear. In this paper, the reactive force field molecular dynamics simulation (ReaxFF-MD) method is used to construct a model of oleic acid methyl ester pyrolysis and combustion system. Further, the chemical conversion kinetics process at high temperatures (2500 K–3500 K) was studied, and a chemical reaction network was drawn. The research results show that the density of the system has almost no effect on the decomposition activation energy of oleic acid methyl ester, and the activation energies of its pyrolysis and combustion processes are 190.02 kJ/mol and 144.89 kJ/mol, respectively. Ethylene, water and carbon dioxide are the dominant and most accumulated products. From the specific reaction mechanism, the main pyrolysis path of oleic acid methyl ester is the breakage of the C-C bond to produce small molecule intermediates, and subsequent transformation of the ester group radical into carbon oxides. The combustion path is the evolution of long-chain alkanes into short-carbon-chain gaseous products, and these species are further burned to form stable CO₂ and H₂O. This study further discusses the microscopic combustion kinetics of biodiesel, providing a reference for the construction of biodiesel combustion models. Based on this theoretical study, the understanding of free radicals, intermediates, and products in the pyrolysis and combustion of biomass can be deepened.

Keywords: methyl oleate; ReaxFF-MD; biodiesel; high temperature chemical conversion

Citation: Wei, Y.; Zhang, X.; Qing, S.; Wang, H. Reaction Mechanism of Pyrolysis and Combustion of Methyl Oleate: A ReaxFF-MD Analysis. *Energies* **2024**, *17*, 3536. <https://doi.org/10.3390/en17143536>

Academic Editor: Gartzzen Lopez

Received: 14 June 2024

Revised: 13 July 2024

Accepted: 15 July 2024

Published: 18 July 2024



Copyright: © 2024 by the authors. Licensee MDPI, Basel, Switzerland. This article is an open access article distributed under the terms and conditions of the Creative Commons Attribution (CC BY) license (<https://creativecommons.org/licenses/by/4.0/>).

1. Introduction

Biodiesel is mainly produced through catalytic hydrogenation of waste vegetable oil and the transesterification reaction between alcohol and vegetable oil. Among them, fatty acid methyl esters, as a common component, can be used as an alternative to traditional fossil fuels [1,2]. Although biodiesels with different components have different physical properties, their combustion characteristics are not inferior to those of traditional diesel, and their carbon emissions are lower [3–6]. Biodiesel usually includes a mixture of various long-chain saturated and unsaturated fatty acid alkyl esters [7,8]. The main fatty acid methyl esters include methyl oleate (C₁₉H₃₆O₂), methyl linoleate (C₁₉H₃₄O₂), methyl linolenate (C₁₉H₃₂O₂), methyl palmitate (C₁₇H₃₄O₂), and methyl stearate (C₁₉H₃₈O₂) [9,10]. Compared with traditional fossil fuels, biodiesel has a wide range of raw material sources, is renewable, has a high fuel calorific value, and has no toxic gas emissions, making it a strong competitor among traditionally available fuel products [11].

As the most important component of biodiesel, methyl oleate has a high cetane number (CN) and low harmful gas emission characteristics [12–14]. Niu et al. [15] studied the

thermal degradation performance of methyl oleate through different degradation and conversion methods and calculated the apparent activation energy. Campbell et al. [16] studied the ignition kinetics mechanism of methyl oleate and measured the shock tube ignition delay time of pure methyl oleate. Soloiu et al. [17] determined the cetane number and apparent heat release rate of methyl oleate and found that the apparent heat release rate of methyl oleate is already similar to that of biodiesel. The above studies confirm the potential of methyl oleate as biodiesel. Wang et al. [18] selected methyl oleate as a model compound of biodiesel and analyzed the thermal transformation behavior under the action of copper slag, which provided a reference for the study of the reaction characteristics of biodiesel alternative fuels. Naik et al. [19] proposed a new reaction mechanism for biodiesel based on the combustion experiments of methyl oleate and methyl stearate. The research shows that methyl oleate has excellent combustion reactivity and advantages as an alternative fuel. However, the existing experimental methods are difficult to fully and comprehensively reveal the $C_{19}H_{36}O_2$ reaction mechanism, and its microscopic reaction network needs to be studied. Therefore, a more detailed exploration of the kinetic mechanism is required.

The Reaction force field Molecular Dynamics (ReaxFF-MD) method, developed by Van Duin et al., describes the formation and transformation of substances based on the atomic level, and is a molecular simulation method for describing chemical reaction processes [20]. Compared with the traditional density functional theory (DFT) method, ReaxFF-MD has the advantages of fast calculation speed and large calculation system while ensuring the accuracy of the calculation [21]. In addition, it is widely used to study the pyrolysis or combustion processes of various substances [22,23]. Liu et al. [24] used ReaxFF-MD to study the isothermal pyrolysis process of polycarbonate, reproduced the experimental pyrolysis products, and verified the reliability of the reaction force field. Zheng et al. [25] simulated the pyrolysis process of palm kernel oil and obtained two different pyrolysis paths of its main component triglycerides at high temperatures. Zhang et al. [26] took RP-3 as the model compound to study the pyrolysis, dehydrogenation and coking processes during its combustion process, and proposed the “core-shell structure” model of coke formation. Goncalves et al. [27] obtained detailed reaction kinetic parameters of the pyrolysis and combustion processes of jet fuel through the ReaxFF force field. The results show that this method can accurately evaluate the species conversion behavior of the combustion system. Wang et al. [28] used molecular dynamics to study the weak oxidation mechanism of methyl in the process of diesel alternative fuel and obtained the complex reaction details. Sun et al. [29] used the ReaxFF-MD method to study the pyrolysis and combustion process of methyl palmitate, obtained its pyrolysis and combustion activation energy, and proposed the reaction mechanism of methyl palmitate. Sui et al. [8] described the mechanism of the effect of double bonds on the formation of long-chain intermediates by analyzing the initial reaction path of methyl linoleate. Li [30] obtained the reaction network of ethyl butyrate under high temperature conditions through the ReaxFF-MD method. Li [31] conducted experiments and employed ReaxFF-MD methods to explore the flame propagation characteristics and reaction mechanism of stearic acid under different conditions. The above research results prove that the ReaxFF-MD method is suitable for exploring the high-temperature transformation process of methyl oleate.

In this paper, the pyrolysis and combustion processes of methyl oleate under different system densities and temperatures are simulated based on the reactive force field molecular dynamics simulation method. By analyzing the high-temperature conversion mechanism and chemical reaction network, the quantitative distribution rules of its main products are obtained, and the chemical conversion process is qualitatively studied. Temperature is the main factor affecting the chemical reactivity and product distribution of methyl oleate, and the activation energy of the combustion reaction is lower than that of the pyrolysis reaction. These results will further enhance our understanding of the mechanism underlying the pyrolysis and combustion process of biodiesel.

2. Models and Methods

In order to investigate the influence of factors such as density, temperature and O_2 content on the reaction process, the pyrolysis and combustion models of $C_{19}H_{36}O_2$ are firstly constructed, and the constructed reaction models are shown in Figure 1. The pyrolysis model includes 30 amorphous $C_{19}H_{36}O_2$ molecules, and the combustion model includes 810 oxygen molecules in addition to 30 methyl oleate molecules. All models have periodic boundary conditions, as shown in Figure 1.

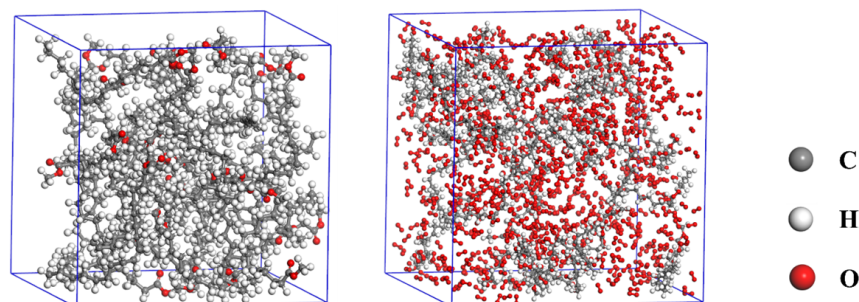


Figure 1. Molecular models of $C_{19}H_{36}O_2$ and $C_{19}H_{36}O_2/O_2$.

It is essential to select an appropriate reactive force field for ReaxFF-MD simulations. In this paper, the C/H/O force field parameters developed by Chenoweth [32] are used to simulate the pyrolysis and combustion processes of $C_{19}H_{36}O_2$, and all calculations are performed in the Large-scale Atomic/Molecular Massively Parallel Simulator (LAMMPS) software [33].

To investigate the reaction mechanisms, the models are first minimized to eliminate atomic overlap, followed by low-temperature relaxation at 300 K for 200 ps using the constant volume–temperature (NVT) ensemble to achieve a stable configuration. During the relaxation process, a time step of 0.1 fs, a Berendsen temperature control method, and a temperature damping constant of 0.1 ps are selected. Subsequently, the NVT ensemble is selected to simulate the pyrolysis and combustion processes of the studied system for 200 ps with a time step of 0.1 fs.

During the simulation, the first step is to conduct a heating and isothermal simulation of methyl oleate, with a heating rate of 20 K/ps, followed by a 100-ps isothermal period at 3000 K to determine the impact of system density. Subsequently, the isothermal combustion process of methyl oleate in an oxygen atmosphere was studied, and the specific details are shown in Table 1. Finally, according to the trajectory file and product file generated from the simulation for post-processing, the reaction pathway is analyzed using the Reac-NetGenerator software [34], and visualization analysis is performed through the OVITO software [35].

Table 1. Simulation details.

| System | Process | T (K) | Duration (ps) | Density (g/cm ³) |
|----------------------------------|------------|-----------------|---------------|------------------------------|
| 30 $C_{19}H_{36}O_2$ | Pyrolysis | 300–3000 + 3000 | 135 + 100 | 0.47 |
| | | | | 0.67 |
| | | | | 0.87 |
| | | | | 1.07 |
| 30 $C_{19}H_{36}O_2$ + 810 O_2 | Combustion | 2000 | 200 | 0.87 |
| | | 2500 | | |
| | | 3000 | | |
| | | 3500 | | |

3. Results and Discussion

3.1. Influence of Density on the Reaction Process

In molecular dynamics simulations, the initial decomposition pathways of methyl oleate mainly include the decomposition of ester groups and C-C bond cleavage, and the different numbers of these molecular species can be used to evaluate the decomposition mechanism of methyl oleate. Figure 2 shows the curves of the number of methyl oleate decomposed at different system densities during pyrolysis. Under the system densities of 0.47 g/cm^3 , 0.67 g/cm^3 , 0.87 g/cm^3 , and 1.07 g/cm^3 , methyl oleate begins to decompose during the heating process. However, from the heating curves, the initial pyrolysis time and temperature of methyl oleate show only small differences. At a heating rate of 20 K/ps , the initial decomposition temperatures are 1578.60 K , 1621.00 K , 1584.40 K , and 1600.00 K , respectively, and the corresponding initial pyrolysis times are 63.93 ps , 66.05 ps , 64.22 ps , and 65.00 ps . From the statistical results, taking the conventional density as a reference, the maximum deviation rate of pyrolysis temperature under different system densities at this temperature rise is only 2.31% , indicating that the system density has little influence on the pyrolysis of methyl oleate under these conditions. From the pyrolysis curves, it can be observed that when the temperature rises above 1500 K , the pyrolysis curves become steeper, and all methyl oleate molecules are consumed within 117.87 ps , with the decomposition temperature at approximately 2657.40 K , and the decomposition rates of different decomposition curves are similar.

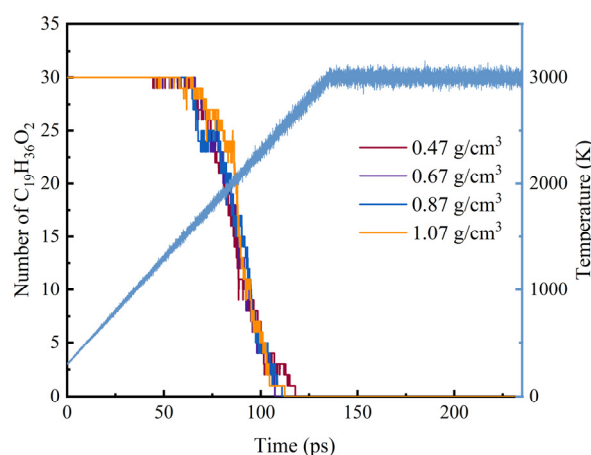


Figure 2. Quantitative changes of $\text{C}_{19}\text{H}_{36}\text{O}_2$ at different system densities.

However, for the combustion process, oxygen effectively promotes the intensity of the forward combustion reaction, and the slope of the number evolution curve of methyl oleate is steeper. Under different system densities, when oxygen participates in the reaction, the initial decomposition times of methyl oleate are 62.24 ps , 56.99 ps , 40.09 ps , and 52.72 ps , and the initial decomposition temperatures are 1544.81 K , 1533.20 K , 1101.80 K , and 1354.20 K , respectively, with the decomposition time being advanced and the decomposition temperature being lowered, as shown in Figure 3. Under the system densities of 0.47 g/cm^3 , 0.67 g/cm^3 , 0.87 g/cm^3 , and 1.07 g/cm^3 , the times for the initial consumption of methyl oleate are 103.66 ps , 93.51 ps , 97.80 ps , and 98.82 ps , respectively.

By comparing the pyrolysis and combustion processes, it can be observed that the decomposition temperature in the combustion process is lower than that in the pyrolysis process. From the curves of the number of methyl oleate, the slopes of the number evolution curves at different system densities are similar, and the distribution of the four curves does not show significant differences. Comprehensive analysis of the pyrolysis and combustion processes at different system densities reveals that for the pyrolysis process, the time range from the start of decomposition to the complete decomposition of the first stage of methyl oleate is within 60 ps to 120 ps , while for the combustion process, it is within 60 ps to 100 ps . The results indicate that for the initial decomposition reaction, the increase in system

density hardly changes the decomposition activation energy. That is, the system density has little influence on the evolution of the initial decomposition quantity of the reactants, which is similar to the influence characteristics of CL-20 [36].

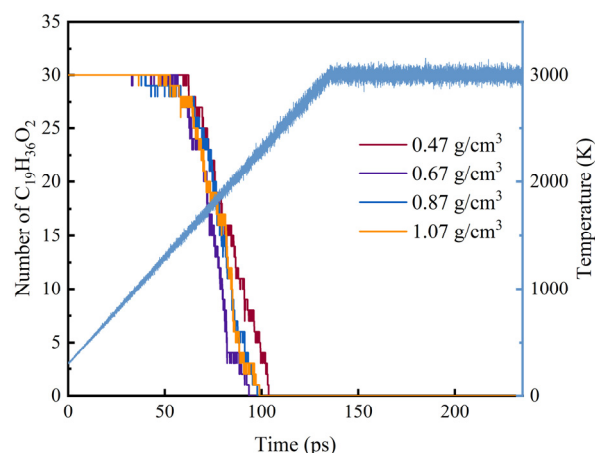


Figure 3. Quantitative changes in the combustion of $C_{19}H_{36}O_2$ at different system densities.

3.2. Based on the ReaxFF-MD Method for Calculating E_a

Figure 4 shows the time evolution and quantity change of $C_{19}H_{36}O_2$ pyrolysis and combustion processes at different temperatures. The decomposition rate of $C_{19}H_{36}O_2$ accelerates with increasing temperature. As shown in Figure 4a,b, during the pyrolysis process, the initial decomposition times of $C_{19}H_{36}O_2$ at 2000 K, 2500 K, 3000 K, and 3500 K are 3.66 ps, 1.55 ps, 0.44 ps and 0.25 ps, respectively. $C_{19}H_{36}O_2$ is completely decomposed at all temperatures, and the total decomposition times are 179.98 ps, 39.25 ps, 4.58 ps and 2.37 ps, respectively. At 3500 K, both the initial decomposition time and the total consumption time are shorter than those at 2000 K.

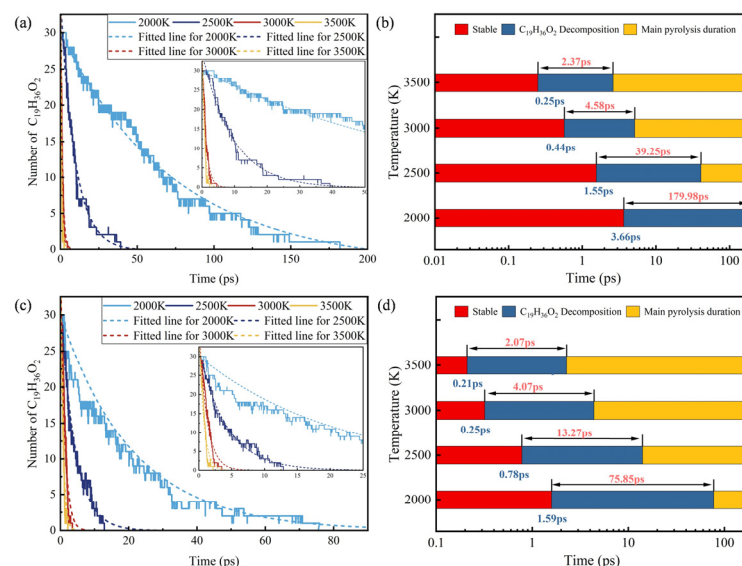


Figure 4. Changes in number of $C_{19}H_{36}O_2$ during the reaction: (a) pyrolysis and (c) combustion, and decomposition times of $C_{19}H_{36}O_2$ (b) pyrolysis and (d) combustion.

In addition, the initial decomposition time and the total consumption time of $C_{19}H_{36}O_2$ in the combustion process are both earlier than those in the pyrolysis process. Especially at 2000 K and 2500 K, the time required for complete decomposition of $C_{19}H_{36}O_2$ in the combustion process is 56.8% and 65.2% shorter than that in the pyrolysis process, respectively. Compared with the above two temperature conditions, the complete decomposition

efficiency at 3000 K and 3500 K is lower. That is, the presence of O_2 shortens the initial decomposition time of $C_{19}H_{36}O_2$ and accelerates the decomposition rate. However, when the temperature rises to 3000 K, the main factor affecting the decomposition of $C_{19}H_{36}O_2$ is temperature, and O_2 is a secondary factor.

To study the reaction kinetics characteristics of $C_{19}H_{36}O_2$, the reaction rate constant k of $C_{19}H_{36}O_2$ is obtained, which is based on the curve of time–number change of $C_{19}H_{36}O_2$. Then, based on the Arrhenius equation, the activation energies, E_a , for the pyrolysis and combustion reactions are calculated. The first-order exponential decay equation is shown in Equation (1).

$$\ln N_0 - \ln N_t = k(t - t_0) \quad (1)$$

where N_0 is the number of $C_{19}H_{36}O_2$ at the initial moment, taking $N_0 = 30$, t_0 is the time when decomposition begins, and N_t is the number of $C_{19}H_{36}O_2$ at time t .

The calculated k_1 and k_2 of $C_{19}H_{36}O_2$ in the pyrolysis and combustion processes were then used to calculate E_a through the Arrhenius equation, as shown in Equation (2).

$$k = A \exp(-E_a/RT) \quad (2)$$

where T is the temperature, R is the gas constant, and A is the pre-exponential factor.

Figure 5 shows the fitting relationship between the reaction rate and temperature of $C_{19}H_{36}O_2$. Compared with the low-vapor-pressure ignition delay experiment of methyl oleate, in which the measured activation energy for the combustion of methyl oleate is 152.36 kJ/mol [37], the activation energies, E_a , for the pyrolysis and combustion processes of $C_{19}H_{36}O_2$ obtained by fitting in this study are 190.02 kJ/mol and 144.89 kJ/mol, respectively, with an error result of 5.2%. This proves the rationality of the model constructed in this paper and the accuracy of the simulation results.

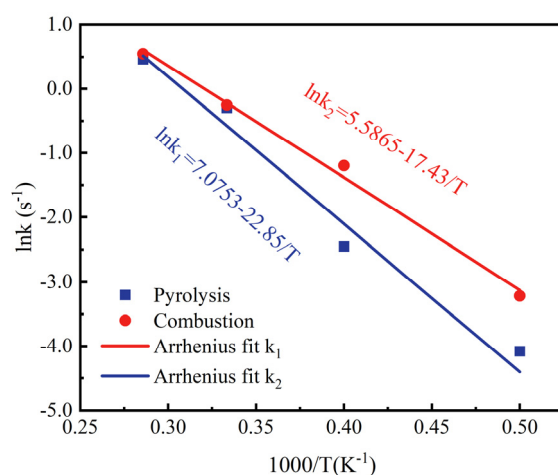


Figure 5. Fitting relationship between the reaction rate and temperature of $C_{19}H_{36}O_2$.

3.3. Influence of Temperature on Products

The main pyrolysis products at different temperatures are shown in Figure 6. It can be seen that the main pyrolysis products of $C_{19}H_{36}O_2$ include C_2H_4 , H_2 , CO_2 and CH_4 , etc. Among them, C_2H_4 is the most dominant product at all four temperatures, and its amount increases rapidly in a short period of time. At 3000 K and 3500 K, the number of C_2H_4 shows a trend of increasing first and then decreasing, while at 2000 K and 2500 K, its number keeps increasing. All in all, the quantity change law of ethylene is characterized by a rapid increase in the early stage, and a decrease in the growth rate when the reaction proceeds to the later stage. The final accumulated quantities of ethylene molecules are 70, 96, 63 and 35, respectively. With the increase in temperature, the reaction activity of ethylene molecules is enhanced, and thus it will further react with other species and be consumed.

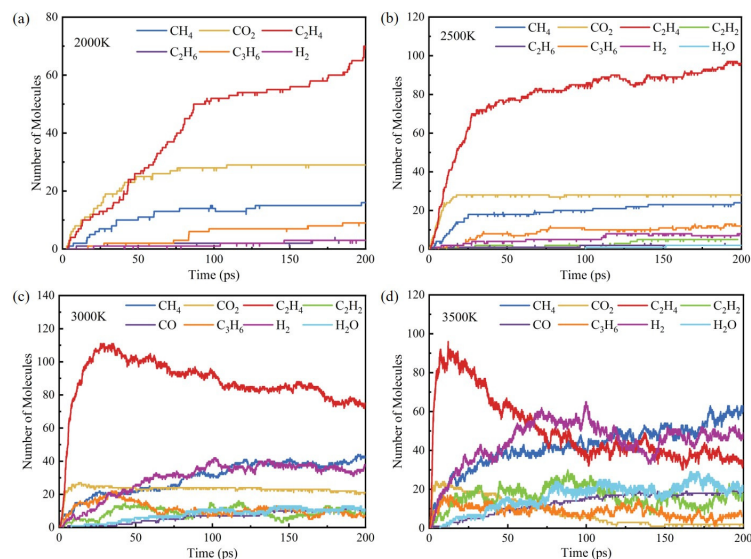


Figure 6. Main pyrolysis products at different temperatures: (a) 2000 K, (b) 2500 K, (c) 3000 K and (d) 3500 K.

CH_4 and C_3H_6 are the main small molecule intermediate products. The number of CH_4 increases gradually with the increase in temperature, from 16 at 2000 K to 60 at 3500 K, presenting an almost four-fold increase. The number of C_3H_6 remains below 20 at all temperatures, indicating that the generated C_3H_6 will further decompose to form other products.

As shown in Figure 7a,b, no H_2O , H_2 and CO products are generated at 2000 K, but as the temperature increases, these products begin to appear and continuously increase. Among them, the change in the number of H_2 is the most obvious, and the numbers are 8, 37 and 47 at 2500 K, 3000 K and 3500 K, respectively. When the simulation proceeds to a certain extent, its number shows a dynamic constant state, that is, the generation and consumption of hydrogen in the middle stage of the reaction should be dynamic. As can be seen from Figure 7c,d, at 3500 K, at the end of the simulation, the number of CO_2 is far less than that of CO , and when the number of CO increases, the number of CO_2 decreases, indicating that more free radical reaction generates CO with a greater probability in the reaction process. It can be seen from Figure 7c,d that at the end of the simulation at 3500 K, the amount of CO is much less than that of CO_2 . As the reaction time elapses and the amount of CO_2 increases, the amount of CO decreases, indicating that not only carbon atoms are oxidized to form CO_2 in this process, but also CO is oxidized.

There are many free radicals, intermediate products and stable products generated during the combustion process of $\text{C}_{19}\text{H}_{36}\text{O}_2$. Figure 7 shows the main combustion products at different temperatures. The main combustion products of $\text{C}_{19}\text{H}_{36}\text{O}_2$ at different temperatures include CH_2O , H_2O , CO_2 and C_2H_4 , etc.

As a typical intermediate product, the characteristic of the number curve of C_2H_4 is to increase first and then decrease, and the higher the temperature, the more obvious the peak characteristics, and the earlier it reaches the peak value. When the temperature is higher than 3000 K, ethylene is rapidly consumed and the number decreases rapidly to 0. The increase in temperature accelerates the decomposition of C_2H_4 , making it fully react in a short period of time.

For CH_2O , its quantity change law is similar to that of C_2H_4 , but shows some differences at different temperatures. At 2000 K and 2500 K, there are two stages. The first stage is the growth stage, and the number of CH_2O keeps increasing; the second stage is the stable stage, and the number of CH_2O fluctuates within a small range. The maximum number of CH_2O at 2000 K is 75. However, as the temperature increases, CH_2O is decomposed or participates in the reaction in large quantities, and its number gradually decreases, and it is

completely consumed at 154.5 ps at 3500 K. The higher the temperature, the smaller the number of CH_2O in the growth and stable stages, and the high temperature promotes the decomposition process.

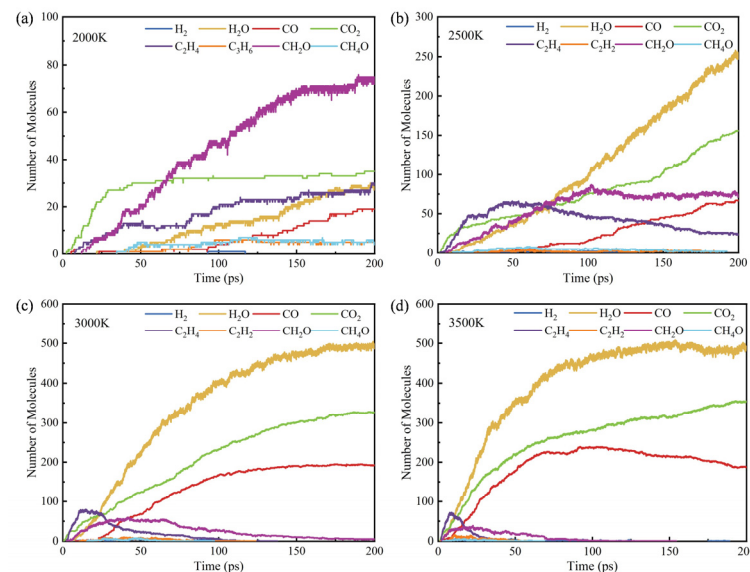


Figure 7. Main combustion products at different temperatures: (a) 2000 K, (b) 2500 K, (c) 3000 K and (d) 3500 K.

Figure 8 shows the distribution of C_2H_4 at different temperatures in the pyrolysis and combustion processes. It can be seen from Figure 8a,b that in the pyrolysis process, there is a residual of C_2H_4 at the end of the simulation at all temperatures, and except at 2000 K, the residual amount of C_2H_4 decreases gradually with the increase in temperature. While in the combustion process, due to the participation of O_2 , the reaction is more violent, and the consumption rate of C_2H_4 greatly increases, so there is less ethylene remaining. At 3000 K and 3500 K, C_2H_4 is completely consumed at 137.69 ps and 51.26 ps, respectively.

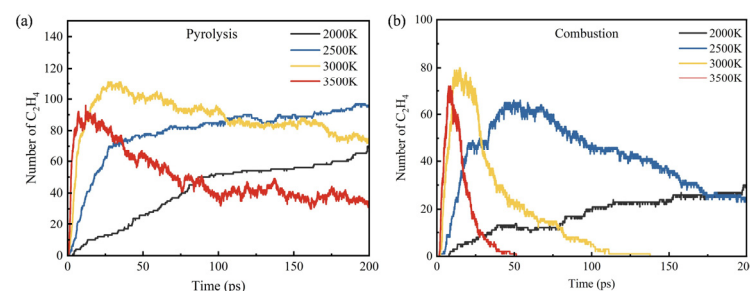


Figure 8. C_2H_4 product distribution at different temperatures: (a) pyrolysis and (b) combustion.

Figure 9 shows the distribution curve of H_2 in the pyrolysis and combustion processes at different temperatures. At lower temperatures, there is less production of H_2 during pyrolysis, which may be due to the short simulation time and insufficient time for the H_2 generation reaction to occur. With the increase in temperature, the number of H_2 shows an increasing trend, with 3, 8, 37 and 47 at 2000 K, 2500 K, 3000 K and 3500 K, respectively. In the combustion process, H_2 is generated at all temperatures, but the quantity is much lower than that in the pyrolysis process, and it is completely consumed before 150 ps. In the combustion process, due to the presence of O_2 , the generated H_2 reacts with O_2 to form stable products H_2O .

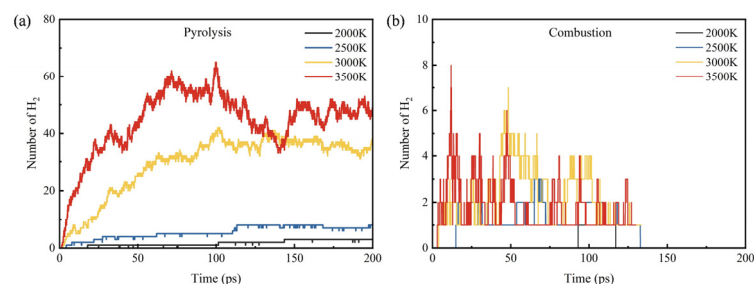


Figure 9. H₂ product distribution at different temperatures: (a) pyrolysis and (b) combustion.

The number distribution of the main combustion products of C₁₉H₃₆O₂ at different temperatures is shown in Figure 10. The number of H₂O is the largest among all the products, and the generation rate gradually increases with the increase in temperature. At 3500 K, the number of H₂O increases rapidly within 50 ps, remains stable at 150 ps, and fluctuates around 480. It can be seen from Figure 10b that the higher the temperature, the faster the generation rate of CH₂O, but the accumulated amount is lower, indicating that CH₂O is consumed in large quantities at high temperatures.

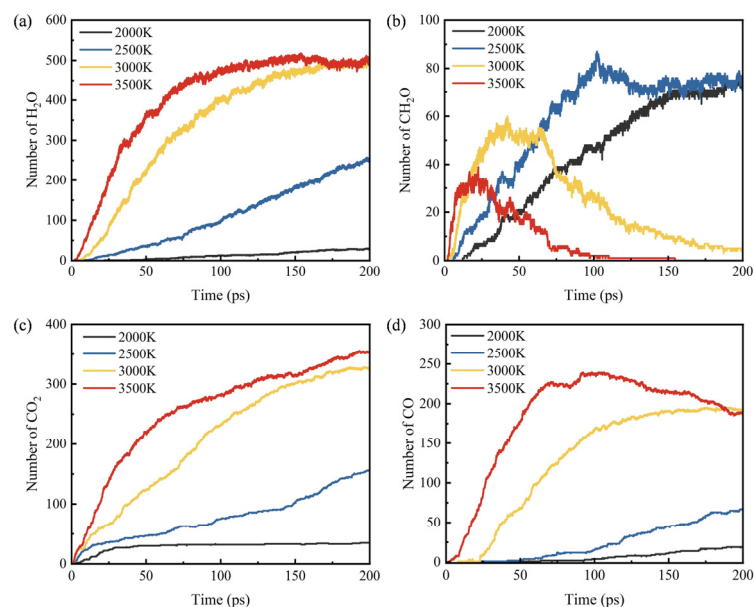


Figure 10. Distribution of major oxidation products of C₁₉H₃₆O₂ combustion: (a) H₂O, (b) CH₂O, (c) CO₂ and (d) CO.

As the most important carbon oxide, the molecular quantity change laws of CO₂ and CO are similar, and the higher the temperature, the more they are generated. The level of CO₂ is relatively stable at 2000 K, but gradually increases with the increase in temperature. In Figure 10d, the higher the temperature, the earlier the generation time of CO and the greater the number. At 3500 K, the level of CO decreases in the later stage of the reaction, which because the consumption rate of CO is greater than the generation rate at too high a temperature, resulting in a large consumption of CO.

3.4. Main Product Reaction Pathways

To further investigate the specific consumption mechanism of methyl oleate, statistics are made on the main production and consumption pathways of the main intermediate and final products. The reaction path diagrams of the main species such as C₂H₄, CH₄, H₂O, CO, and CO₂ are drawn, as shown in Figure 11. From the main paths and proportions, it is found that C₂H₄ is most likely to interact with free ·H, regardless of its formation or consumption, and this path accounted for more than 60%. Under high temperature conditions, the

intermediate radicals decomposed from methyl oleate are extremely unstable, and bond-forming reactions occurred under the collision of free $\cdot\text{H}$, generating ethylene and other species. In this process, due to the relatively high bond energy of $\text{C}=\text{C}$, the collision to form double bonds became the main formation pathway of ethylene.

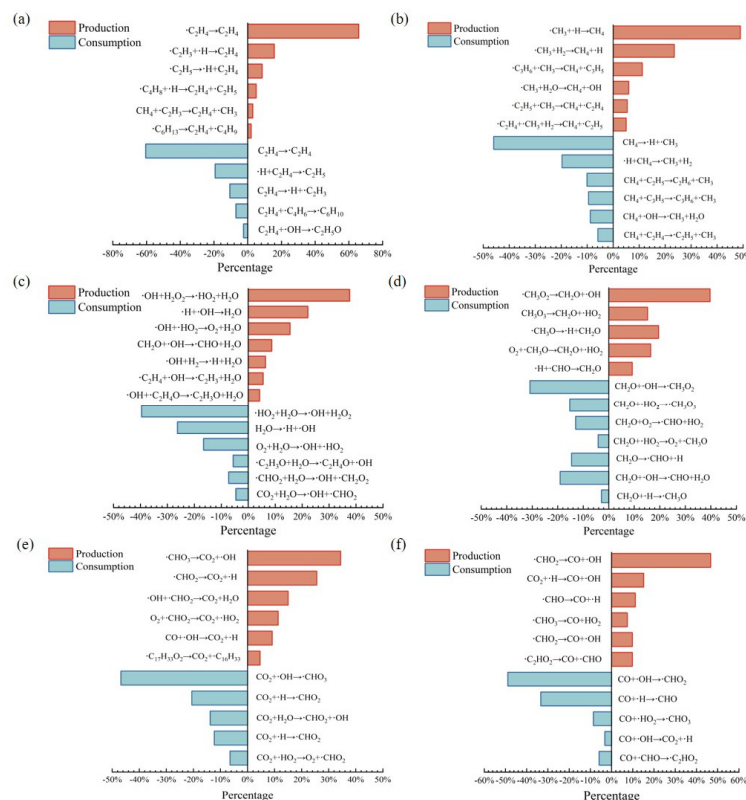


Figure 11. Main product reaction pathways: (a) C_2H_4 , (b) CH_4 , (c) H_2O , (d) CH_2O , (e) CO_2 and (f) CO .

As the main intermediate product, the main consumption mode of formaldehyde is dehydroxylation reaction ($\cdot\text{CH}_2\text{O}_2 \rightarrow \text{CH}_2\text{O} + \text{OH}$), which accounts for approximately 39.7%. The consumption process is mainly a redox reaction with oxygen-containing radicals, and more than half of the consumption pathways are this reaction.

The generation of carbon oxides involves the redox reaction between the $\text{C}=\text{O}$ bond group and oxygen-containing free radicals. The main generation path of CO is the $\cdot\text{CH}_2\text{O}$ radical produced by the decomposition of methyl oleate during the combustion process. These free radical groups lose hydrogen atoms to generate the reducing gas CO . In addition to the similar path to the generation of CO , the formation of CO_2 also includes the stepwise decomposition of methyl oleate ($\text{C}_{19}\text{H}_{36}\text{O}_2 \rightarrow \text{C}_{17}\text{H}_{31}\text{COOH} + \text{CH}_4 \rightarrow \text{CO}_2 + \text{H}_2\text{O}$, where the alkane or acid substances produced by the decomposition of methyl oleate react with O_2 to produce CO_2), and the interaction between free hydroxyl groups and $\cdot\text{CH}_2\text{O}$ radicals. In general, the generation path of CO_2 is relatively more, and it may be generated from carboxyl radicals, hydroxyl radicals, and aldehyde radicals.

There are two main pathways for the generation of the final product H_2O . One is the reduction reaction of unstable peroxides, that is, the interaction between $\cdot\text{OH} + \cdot\text{H}_2\text{O}_2$, and the other is the typical formation reaction of water, that is, the bond formation between free hydrogen and free $\cdot\text{OH}$. The proportions of these two pathways in this process are relatively high, accounting for 59.7% of all generation reactions.

3.5. $\text{C}_{19}\text{H}_{36}\text{O}_2$ Reaction Mechanism

Based on the ReacNetGenerator script [34], the reaction network of the pyrolysis and combustion processes of methyl oleate is analyzed and plotted, as shown in Figure 12.

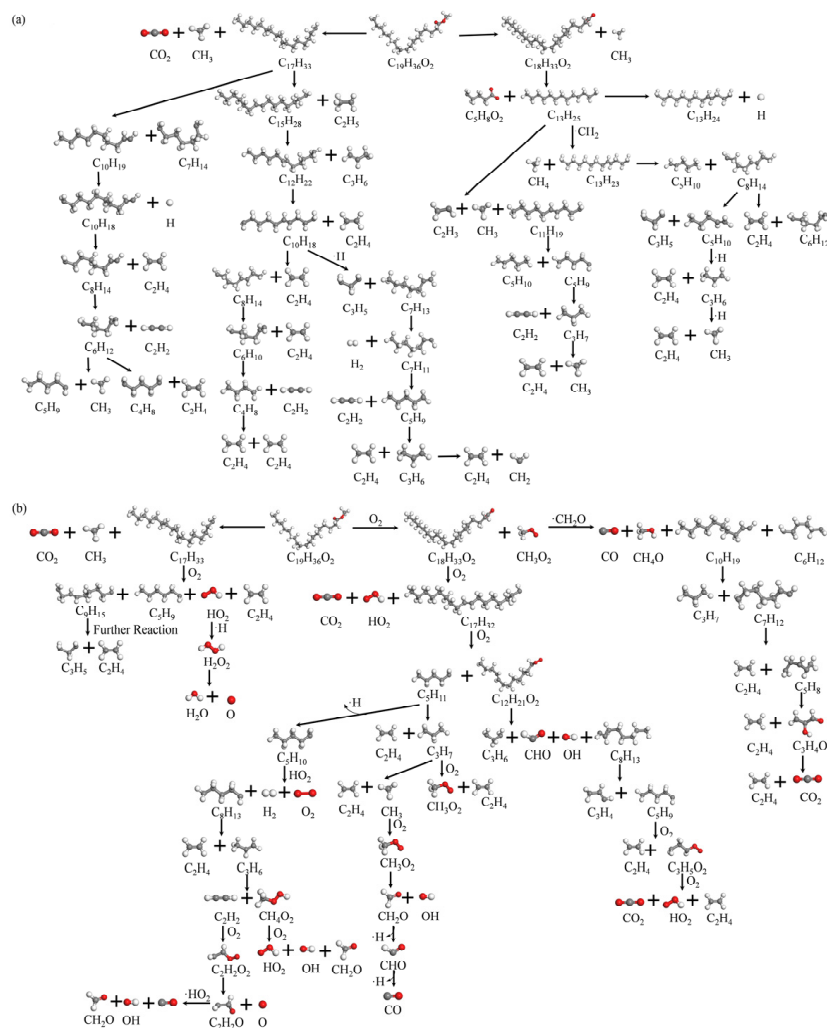


Figure 12. Reaction mechanism of $C_{19}H_{36}O_2$: (a) Pyrolysis, (b) Combustion.

It can be seen from Figure 12a that the initial pyrolysis path of methyl oleate starts with the cleavage of the C-C bond. Due to the position of the ester group, methyl oleate may have two main pyrolysis methods: (1) The C-C bond at the ester group position is broken, and the first bond-breaking of methyl oleate produces $\cdot\text{C}_{18}\text{H}_{33}\text{O}_2$ and $\cdot\text{CH}_3$. These two intermediate groups are unstable and will further react with other $\cdot\text{H}$ to produce unstable intermediate products including methane, acids, alcohols, etc. (2) The C-C bond of $\text{R-CH}_2\text{CH}_3$ at the other end is broken, first producing alkanes and another ester substance. Further, the substance containing the ester group continues to decompose or is consumed by reacting with $\cdot\text{H}$. This consumption pathway involves the multi-step interaction of various oxygen-containing groups, and the reaction network gradually becomes more complex, causing the long-chain macromolecular products to gradually transform into hydrocarbons and carbon oxides.

For the combustion process, the addition of O_2 makes the whole reaction network more complex, although the bond-breaking process in the initial stage is similar, as shown in Figure 12b. The high-temperature combustion process will produce a large number of unstable intermediates, and the decomposition reaction proceeds more quickly and completely. Moreover, oxygen further enhances the reactivity of methyl oleate. As a result, the intermediate species in the combustion process are mainly short carbon chain alkanes and carboxylic acid substances. The results show that methyl oleate first breaks bonds to produce oleic acid and methane, and oleic acid further breaks bonds to generate gaseous species (C_{0-5}). Subsequently, O_2 takes hydrogen from the hydrocarbon groups to generate

stable compounds H_2O , and the remaining carbon combines with oxygen to evolve into CO_2 and CO . In addition, the reaction of methanol and formaldehyde with $\cdot\text{OH}$ to generate water is also observed, which is one of the main production pathways of H_2O in the combustion process.

4. Conclusions

In this paper, the ReaxFF method is used to study the pyrolysis and combustion processes of methyl oleate. Taking density, temperature, and heating rate as the main considerations, the reaction mechanisms of the pyrolysis and combustion processes are explored. The main conclusions are as follows:

- (1) The initial pyrolysis path of methyl oleate is the breaking of the C-C bond, generating large molecular intermediates and methane. Subsequently, long-chain species continue to decompose into small molecule gaseous substances, and finally evolve to produce species such as methane and ethylene. In contrast, the intermediate products generated during combustion are mainly short carbon chain gases, which further combust to generate stable CO_2 and H_2O .
- (2) During the pyrolysis and combustion processes, ethylene, water, and carbon dioxide are the main products with the highest cumulative amounts. As the reaction process progresses, the amount of ethylene first increases rapidly, and then rapidly decreases, while the amounts of water and carbon dioxide keep increasing.
- (3) The pyrolysis and combustion processes are simulated at temperatures of 2000 K, 2500 K, 3000 K, and 3500 K. The results show that the chemical reactivity of methyl oleate is stronger in the combustion process. The activation energy of the pyrolysis process is 190.02 kJ/mol, and the combustion activation energy is 144.89 kJ/mol.
- (4) This study is dedicated to the development of methyl oleate. Through in-depth research, a kinetic model for the high-temperature conversion of methyl oleate has been initially established, which will enhance our understanding of the thermochemical conversion of biodiesel fuels.

Author Contributions: Y.W.: Conceptualization, Data curation, Software, Validation, Investigation, Formal analysis, Writing—original draft. X.Z.: Conceptualization, Funding acquisition, Resources, Supervision, Writing—review and editing. S.Q.: Funding acquisition, Investigation. H.W.: Software, Validation. All authors have read and agreed to the published version of the manuscript.

Funding: This work is supported by National Natural Science Foundation of China under Contract (No. 51966005); Yunnan Fundamental Research Projects (No. 202101AT070120, 202301AT070469); Yunnan Major Scientific and Technological Projects (No. 202202AG050002).

Data Availability Statement: Data cannot be shared publicly, because data from this study may contain sensitive information about the companies.

Acknowledgments: The authors are grateful to reviewers for their attention and comments on our work, which makes our revision more clear and complete.

Conflicts of Interest: The authors declare no conflicts of interest.

References

1. Knothe, G.; Razon, L.F. Biodiesel fuels. *Prog. Energy Combust. Sci.* **2017**, *58*, 36–59. [\[CrossRef\]](#)
2. Glisic, S.B.; Pajnik, J.M.; Orlović, A.M. Process and techno-economic analysis of green diesel production from waste vegetable oil and the comparison with ester type biodiesel production. *Appl. Energy* **2016**, *170*, 176–185. [\[CrossRef\]](#)
3. Ando, S.; Wu, Y.; Nakaya, S.; Tsue, M. Droplet combustion behavior of oxidatively degraded methyl laurate and methyl oleate in microgravity. *Combust. Flame* **2020**, *214*, 199–210. [\[CrossRef\]](#)
4. Zhou, W.; Wang, Z.; Liang, Y.; Zhang, X.; Yu, L.; Lu, X. The effect of the unsaturation degree on the gas-phase autoignition of methyl oleate and methyl linoleate: Experimental and modeling study. *Combust. Flame* **2024**, *263*, 113381. [\[CrossRef\]](#)
5. Ahmad, T.; Danish, M.; Kale, P.; Geremew, B.; Adeloju, S.B.; Nizami, M.; Ayoub, M. Optimization of process variables for biodiesel production by transesterification of flaxseed oil and produced biodiesel characterizations. *Renew. Energy* **2019**, *139*, 1272–1280. [\[CrossRef\]](#)

6. Bhatia, S.K.; Bhatia, R.K.; Jeon, J.; Pugazhendhi, A.; Awasthi, M.K.; Kumar, D.; Kumar, G.; Yoon, J.; Yang, G. An overview on advancements in biobased transesterification methods for biodiesel production: Oil resources, extraction, biocatalysts, and process intensification technologies. *Fuel* **2021**, *285*, 119117. [\[CrossRef\]](#)
7. Herbinet, O.; Pitz, W.J.; Westbrook, C. Detailed chemical kinetic mechanism for the oxidation of biodiesel fuels blend surrogate. *Combust. Flame* **2010**, *157*, 893–908. [\[CrossRef\]](#)
8. Sui, M.; Li, F.; Wang, S.; Wang, H. Molecular dynamics simulation and experimental research on the oxidation reaction of methyl linoleate at low oxygen and high temperature. *Fuel* **2021**, *305*, 121478. [\[CrossRef\]](#)
9. Soloiu, V.; Moncada, J.D.; Gaubert, R.; Knowles, A.; Molina, G.; Ilie, M.; Harp, S.; Wiley, J.T. Reactivity Controlled Compression Ignition combustion and emissions using n-butanol and methyl oleate. *Energy* **2018**, *165*, 911–924. [\[CrossRef\]](#)
10. Zhou, W.; Liang, Y.; Pei, X.; Zhang, Y.; Yu, L.; Lu, X. Autoignition of methyl palmitate in low to intermediate temperature: Experiments in rapid compression machine and kinetic modeling. *Combust. Flame* **2023**, *249*, 112619. [\[CrossRef\]](#)
11. Jiaqiang, E.; Liu, T.; Yang, W.; Deng, Y.; Gong, J. A skeletal mechanism modeling on soot emission characteristics for biodiesel surrogates with varying fatty acid methyl esters proportion. *Appl. Energy* **2016**, *181*, 322–331.
12. Demirbas, A. Progress and recent trends in biodiesel fuels. *Energy Convers. Manag.* **2009**, *50*, 14–34. [\[CrossRef\]](#)
13. Knothe, G. Biodiesel and renewable diesel: A comparison. *Prog. Energy Combust. Sci.* **2010**, *36*, 364–373. [\[CrossRef\]](#)
14. Türck, J.; Schmitt, F.; Anthofer, L.; Türck, R.; Ruck, W.; Krah, J. Extension of Biodiesel Aging Mechanism—the Role and Influence of Methyl Oleate and the Contribution of Alcohols Through the Use of SolketaL. *ChemSusChem* **2023**, *16*, e202300263. [\[CrossRef\]](#) [\[PubMed\]](#)
15. Niu, S.; Zhou, Y.; Yu, H.; Lu, C.; Han, K. Investigation on thermal degradation properties of oleic acid and its methyl and ethyl esters through TG-FTIR. *Energy Convers. Manag.* **2017**, *149*, 495–504. [\[CrossRef\]](#)
16. Campbell, M.F.; Davidson, D.F.; Hanson, R.K. Ignition delay times of methyl oleate and methyl linoleate behind reflected shock waves. *Proc. Combust. Inst.* **2013**, *34*, 419–425. [\[CrossRef\]](#)
17. Soloiu, V.; Knowles, A.R.; Carapia, C.E.; Moncada, J.D.; Wiley, J.T.; Kilpatrick, M.; Williams, J.; Rahman, M.; Ilie, M. n-Butanol and Oleic Acid Methyl Ester, Combustion and NVH Characteristics In Reactivity Controlled Compression Ignition. *Energy* **2020**, *207*, 118183. [\[CrossRef\]](#)
18. Wang, Y.; Zhang, F.; Hu, J.; Yang, S.; Liu, H.; Wang, H. Investigation of Pyrolysis Characteristics and Product Evolution Behavior of Methyl Oleate under the Effect of Copper Slag. *Catal. Lett.* **2024**. [\[CrossRef\]](#)
19. Naik, C.V.; Westbrook, C.K.; Herbinet, O.; Pitz, W.J.; Mehl, M. Detailed chemical kinetic reaction mechanism for biodiesel components methyl stearate and methyl oleate. *Proc. Combust. Inst.* **2011**, *33*, 383–389. [\[CrossRef\]](#)
20. Duin, A.C.T.; Dasgupta, S.; Lorant, F.; Goddard, W.A. ReaxFF: A Reactive Force Field for Hydrocarbons. *J. Phys. Chem. A* **2001**, *105*, 9396–9409. [\[CrossRef\]](#)
21. Baltin, R. One-dimensional hypervirial theorems in density functional theory. *Phys. Lett. A* **1985**, *113*, 121–125. [\[CrossRef\]](#)
22. Zhang, Y.; Li, W.; Pei, Q.; Zhang, X.; Zhou, Z.; Xu, S.; Lan, Y.; Jiao, F.; Shi, X.; Xu, S.; et al. Effect of stearic acid coating on the flame propagation and reaction mechanism of AlH₃. *Fuel* **2024**, *358*, 130140. [\[CrossRef\]](#)
23. Zhao, T.; Li, T.; Xin, Z.; Zou, L.; Zhang, L. A ReaxFF-Based Molecular Dynamics Simulation of the Pyrolysis Mechanism for Polycarbonate. *Energy Fuels* **2018**, *32*, 2156–2162. [\[CrossRef\]](#)
24. Liu, Q.; Liu, S.; Lv, Y.; Hu, P.; Huang, Y.; Kong, M.; Li, G. Atomic-scale insight into the pyrolysis of poly-carbonate by ReaxFF-based reactive molecular dynamics simulation. *Fuel* **2021**, *287*, 119484. [\[CrossRef\]](#)
25. Zheng, H.; Wang, Z.; Yang, T.; Yao, W.; Cai, S.; Li, X.; Liu, C.; Yang, E. Investigation on pyrolysis mechanism of palm olein and the effect of moisture on its pyrolysis. *J. Mol. Liq.* **2021**, *339*, 116824. [\[CrossRef\]](#)
26. Zhang, H.; Li, W.; Nian, Y.; Liu, M.; Zhang, J.; Han, Y. Insights into the pyrolytic coking process of RP-3 fuel from ReaxFF molecular dynamics. *Chem. Eng. Sci.* **2024**, *291*, 119935. [\[CrossRef\]](#)
27. Goncalves, R.; Iha, B.; Rocco, J. Reactive molecular dynamics of pyrolysis and combustion of alternative jet fuels: A ReaxFF study. *Fuel* **2022**, *310*, 122157. [\[CrossRef\]](#)
28. Wang, L.; Liu, Y.; Wang, J.; Li, X.; Ma, J. Effect of CO₂ and methyl groups reaction kinetics on the ignition and combustion of diesel surrogate fuel: Part I. Reaction mechanisms. *Fuel* **2023**, *351*, 128984. [\[CrossRef\]](#)
29. Sun, H.; Zhang, X.; Liu, H.; Li, J.; Wang, H. Pyrolysis and combustion reaction mechanisms of methyl palmitate with ReaxFF-MD method. *Comput. Theor. Chem.* **2024**, *1231*, 114446. [\[CrossRef\]](#)
30. Li, J.; Zhang, X.; Zhang, A.; Wang, H. ReaxFF based molecular dynamics simulation of ethyl butyrate in pyrolysis and combustion. *Chem. Eng. Sci.* **2024**, *284*, 119528. [\[CrossRef\]](#)
31. Li, W.; Zhang, X.; Liu, R.; Xu, S.; Xu, S. Thermal decomposition, flame propagation, and combustion reactions behaviours of stearic acid by experiments and molecular dynamic simulation. *Chem. Eng. J.* **2023**, *461*, 141906. [\[CrossRef\]](#)
32. Chenoweth, K.; Van, D.; Goddard, W.A. ReaxFF Reactive Force Field for Molecular Dynamics Simulations of Hydrocarbon Oxidation. *J. Phys. Chem. A* **2008**, *112*, 1040–1053. [\[CrossRef\]](#)
33. Plimpton, S. Fast Parallel Algorithms for Short-Range Molecular Dynamics. *J. Comput. Phys.* **1995**, *117*, 1–19. [\[CrossRef\]](#)
34. Zeng, J.; Cao, L.; Chin, C.; Ren, H.; Zhang, H.; Zhu, T. ReacNetGenerator: An automatic reaction network generator for reactive molecular dynamics simulations. *Phys. Chem. Chem. Phys.* **2020**, *22*, 683–691. [\[CrossRef\]](#)
35. Stukowski, A. Visualization and analysis of atomistic simulation data with OVITO—the Open Visualization Tool. *Model. Simul. Mater. Sci. Eng.* **2010**, *18*, 015012. [\[CrossRef\]](#)

36. Wang, F.; Chen, L.; Geng, D.; Lu, J.; Wu, J. Effect of density on the thermal decomposition mechanism of ϵ -CL-20: A ReaxFF reactive molecular dynamics simulation study. *Phys. Chem. Chem. Phys.* **2018**, *20*, 22600–22609. [[CrossRef](#)] [[PubMed](#)]
37. Campbell, M.F.; Davidson, D.F.; Hanson, R.K. Ignition delay times of very-low-vapor-pressure biodiesel surrogates behind reflected shock waves. *Fuel* **2014**, *126*, 271–281. [[CrossRef](#)]

Disclaimer/Publisher’s Note: The statements, opinions and data contained in all publications are solely those of the individual author(s) and contributor(s) and not of MDPI and/or the editor(s). MDPI and/or the editor(s) disclaim responsibility for any injury to people or property resulting from any ideas, methods, instructions or products referred to in the content.